10724 *Biochemistry* **2009,** *48,* 10724–10732
DOI: 10.1021/bi9012935

BIOCHEMISTRY
including biophysical chemistry & molecular biology
Article

The Second Cu(II)-Binding Site in a Proton-Rich Environment Interferes with the Aggregation of Amyloid-β(1−40) into Amyloid Fibrils[†]

Sangmi Jun, Joel R. Gillespie, Byong-kyu Shin, and Sunil Saxena*

Department of Chemistry, University of Pittsburgh, Pittsburgh, Pennsylvania 15260

Received July 27, 2009; Revised Manuscript Received September 23, 2009

ABSTRACT: The overall morphology and Cu(II) ion coordination for the aggregated amyloid-β(1−40) [Aβ(1−40)] in *N*-ethylmorpholine (NEM) buffer are affected by Cu(II) ion concentration. This effect is investigated by transmission electron microscopy (TEM), atomic force microscopy (AFM), and electron spin echo envelope modulation (ESEEM) spectroscopy. At lower than equimolar concentrations of Cu(II) ions, fibrillar aggregates of Aβ(1−40) are observed. At these concentrations of Cu(II), the monomeric and fibrillar Aβ(1−40) ESEEM data indicate that the Cu(II) ion is coordinated by histidine residues. For aggregated Aβ(1−40) at a Cu(II):Aβ molar ratio of 2:1, TEM and AFM images show both linear fibrils and granular amorphous aggregates. The ESEEM spectra show that the multi-histidine coordination for Cu(II) ion partially breaks up and becomes exposed to water or exchangeable protons of the peptide at a higher Cu(II) concentration. Since the continuous-wave electron spin resonance results also suggest two copper-binding sites in Aβ(1−40), the proton ESEEM peak may arise from the second copper-binding site, which may be significantly involved in the formation of granular amorphous aggregates. Thioflavin T fluorescence and circular dichroism experiments also show that Cu(II) inhibits the formation of fibrils and induces a nonfibrillar β-sheet conformation. Therefore, we propose that Aβ(1−40) has a second copper-binding site in a proton-rich environment and the second binding Cu(II) ion interferes with a conformational transition into amyloid fibrils, inducing the formation of granular amorphous aggregates.

Amyloid-β (Aβ)[1] peptide, a small peptide that is composed of 39−43 amino acids, is the main constituent of amyloid deposits found in Alzheimer's disease (AD) (*1*). This peptide exists as a normal soluble random coil and undergoes a conformational transition to an insoluble aggregated, fibrillar β-sheet-rich form. It is believed that the progression of AD is correlated with the Aβ intermediates rather than the amyloid plaques (*1*−*5*) and that Cu(II) stabilizes the neurotoxic early-stage intermediates of Aβ (*6*−*8*). Since this neurotoxicity is dependent partly on the state of aggregation in Aβ, one of the goals in Aβ research is focused on characterizing the copper coordination, which can be involved in promoting (*9*) or inhibiting (*7*, *8*, *10*) amyloid fibril formation.

Electron spin resonance (ESR) spectroscopy has shown that Cu(II) is coordinated with histidine residues in the flexible N-terminal region of Aβ. A smaller fragment, Aβ(1−16), has been considered as a suitable model for investigation of Cu(II) ion coordination (*11*, *12*). The peptide, Aβ(1−16), is not aggregated at physiological pH and is traditionally believed to have a copper coordination geometry identical to that of longer, fibril-forming peptides, Aβ(1−40) and Aβ(1−42). We have used isotopic ^{15}N-labeled peptides to demonstrate that the copper-binding site in Aβ(1−16) is coordinated by all three histidine residues (H6, H13, and H14), providing three nitrogen donors to the Cu(II) ion (*13*). Barnham and co-workers have used multi-frequency continuous-wave (CW) ESR spectroscopy to resolve the superhyperfine interaction between the Cu(II) ion and the ligand nuclei of Aβ via selective ^{15}N labeling of specific ligand nuclei. They have also demonstrated two different 3N1O Cu(II) coordination environments involving D1, H6, H13, or H14 in Aβ(1−16) (*14*). However, the longer peptide, Aβ(1−40), includes Aβ(17−21), which is known to be crucial for fibril formation (*15*−*19*). In recent reports, there has been evidence of additional binding sites in longer sequences of Aβ. In particular, Viles and co-workers reported that Aβ(1−28) has two copper-binding sites for a single peptide (*20*) and, recently, demonstrated that two copper-binding sites are present in Aβ(1−42) in a water/methanol mixture (80:20, v/v) (*12*). Bush and co-workers also demonstrated two cooperative copper-binding sites in Aβ(1−40) at pH 7.4 (*21*). Intriguingly, Aβ(1−40) forms granular amorphous aggregates instead of amyloid fibrils at greater than equimolar Cu(II) ion concentrations (*22*, *23*).

In this study, we suggest two copper-binding sites in the Aβ(1−40) aggregates and provide evidence that the second copper-binding site interferes with the conformational transition into amyloid fibrils. By preparing aggregates at different Cu(II) concentrations, we systematically examine different morphological species of Aβ(1−40), such as monomers, fibrils, and amorphous aggregates, by a variety of spectroscopic and imaging techniques. We demonstrate that greater than equimolar Cu(II) concentrations disrupt the formation of regular amyloid fibrils in

[†]The research was supported by National Science Foundation (NSF) CAREER Grant MCB 0346898 and NSF Grant MCB 0842956.

*To whom correspondence should be addressed. Phone: (412) 624-8680. Fax: (412) 624-8611. E-mail: sksaxena@pitt.edu.

[1]Abbreviations: Aβ, amyloid-β; NEM, *N*-ethylmorpholine; TEM, transmission electron microscopy; AFM, atomic force microscopy; ESEEM, electron spin echo envelope modulation; AD, Alzheimer's disease; CW, continuous-wave; ESR, electron spin resonance; ThT, thioflavin T; CD, circular dichroism; HYSCORE, hyperfine sublevel correlation; NQI, nuclear quadrupole interaction; DQ, double-quantum.

 Published on Web 10/13/2009

favor of granular amorphous aggregates based on transmission electron microscopy (TEM) and atomic force microscopy (AFM) images, reduced thioflavin T (ThT) fluorescence emission, and alterations of the far-UV circular dichrosim (CD) spectrum of the peptide. The electron spin echo envelope modulation (ESEEM) spectra for different aggregated stages of Aβ(1−40) in *N*-ethylmorpholine (NEM) buffer suggest that the copper coordination environments of monomers and mature fibrils are identical (*12*, *24*). On the other hand, distinct differences between the copper coordination environment of monomers and amorphous aggregates of Aβ(1−40) exist. The aggregates of Aβ(1−40) have a second copper-binding site, which is exposed to a proton-rich environment. Potentially, this site disrupts protein−protein interactions that lead to formation of fibrils.

MATERIALS AND METHODS

Sample Preparation. Aβ(1−40) (DAEFRHDSGYEVHHQKLVFFAEDVGSNKGAIIGLMVGGVV) was synthesized at the Molecular Medicine Institute, University of Pittsburgh, using standard fluorenylmethoxycarbonyl chemistry. Aβ(1−40) was purified by high-performance liquid chromatography and characterized by mass spectrometry. The peptide was dissolved in 1% NH_4OH, and the pH value was adjusted to 7.4 with hydrochloric acid. The Aβ(1−40) solution was diluted to the final concentration of 300 μM with a pH 7.4 buffer solution containing 50 mM NEM and 25% (v/v) glycerol. Isotopically enriched (98.6%) $^{63}CuCl_2$ was purchased from Cambridge Isotope Laboratory (Andover, MA), and a Cu(II) solution was prepared in the same NEM buffer. The enriched isotope was used to minimize inhomogeneous broadening of the Cu(II) ESR spectra. To prepare aggregates, Aβ(1−40) was incubated at 37 °C for several days in the presence of an appropriate Cu(II) concentration.

Electron Spin Resonance Spectroscopy. For pulsed ESR experiments, 150 μL of peptide sample was transferred into a quartz tube with an inner diameter of 3 mm. The experiments were performed on a Bruker EleXsys E580 X-band CW/Pulse ESR spectrometer equipped with a Bruker ER4118X-MD5 dielectric ring resonator. The temperature was controlled using an Oxford ITC503 temperature controller and an Oxford ER 4118CF gas flow cryostat.

Three-pulse ESEEM spectra of Aβ(1−40) were recorded at 20 K by using a $\pi/2-\tau-\pi/2-T-\pi/2$ pulse sequence with a $\pi/2$ pulse width of 16 ns. The first pulse separation, τ, was set at 200 ns, and the second pulse separation, T, was varied from 400 ns with a step size of 16 ns for a total of 1024 points with 100 averages collected per point. The unwanted signals were eliminated by a four-step phase cycle (*25*, *26*). The data were baseline-corrected and Fourier-transformed to produce the ESEEM spectra. The magnitude of the FT data is shown for all ESEEM spectra.

Hyperfine sublevel correlation (HYSCORE) experiments were also performed with Aβ(1−40) at 20 K by using a $\pi/2-\tau-\pi/2-t_1-\pi-t_2-\pi/2$ pulse sequence with $\pi/2$ and π pulse widths of 16 and 32 ns, respectively. The first pulse separation, τ, was set at 200 ns, and both the second and third pulse separations, t_1 and t_2, respectively, were varied from 200 ns with a step size of 16 ns and 100 averages per point. The final data consisted of 256 points in both t_1 and t_2. The data were baseline-corrected, zero-filled to 512 points, and Fourier-transformed to produce the HYSCORE spectra.

For CW ESR experiments, 30 μL of suspended aggregated peptide was transferred into a quartz tube with an inner diameter of 2 mm (Vitrocom, Mountain Lakes, NJ). All CW ESR spectra were recorded at 80 K with a microwave power of 0.1993 mW, a modulation amplitude of 4 G, a time constant of 40.96 ms, a conversion time of 81.92 ms, and a sweep width of 2000 G.

Thioflavin T Fluorescence Assays. To determine the Aβ-(1−40) fibril growth end points, fluorescence measurements were performed on a HORIBA Jobin Yvon FluoroMax-3 fluorescence spectrometer at an excitation of 440 nm (bandwidth of 5 nm) and emission of 485 nm (bandwidth of 5 nm). A 3 μM ThT solution at pH 8.6 was prepared by dissolving solid ThT (Acros Organics USA, Morris Plains, NJ) in a 50 mM glycine-NaOH buffer (*27*) and stored in a brown bottle to prevent degradation by light. A 13 μL aliquot of the 300 μM Aβ(1−40) solution in the presence of a range of Cu(II) ion concentrations was added to 3 mL of the ThT solution. The sample was placed in a quartz cell with a path length of 1 cm (NSG Precision Cells Inc., Farmingdale, NY) for the measurements.

Circular Dichroism Spectroscopy. The β-sheet conformation of Aβ(1−40) was monitored with CD spectroscopy. The Aβ(1−40) sample was diluted to a final concentration of 28 μM with NEM buffer. Spectra were recorded on an AVIV model 202 circular dichroism spectrometer over the wavelength range of 198−270 nm with a step size of 1 nm, a 1 nm bandwidth, and a scan rate of 2 nm/s. The temperature was fixed at 25 °C using the temperature control. The samples contained 400 μL of the peptide solution in a 0.1 cm path length quartz cuvette. The background was subtracted from each spectrum, but no additional filtering or noise reduction was applied.

Transmission Electron Microscopy. Peptide samples were prepared on 200 mesh copper grids coated with Formvar support films stabilized with a layer of carbon (Ted Pella, Inc., Redding, CA). Samples were applied either with a jet sprayer or by the droplet method (*28*) and were negatively stained with a solution of 1% uranyl acetate. Images were collected with a FEI Morgagni 268 transmission electron microscope operating at 80 keV at the Department of Biological Sciences (University of Pittsburgh) or a JEOL JEM-2100F high-resolution field emission transmission electron microscope operating at 200 keV at the Peterson Institute for Nanoscience Nanoscale Fabrication and Characterization Facility.

Atomic Force Microscopy. Each of the Aβ(1−40) samples was diluted to ~1 or 2 μM with deionized water in an Eppendorf tube, and aliquots of 5 μL were removed from the diluted solution and placed on a freshly cleaved mica surface and air-dried. All images were obtained under ambient conditions with a Veeco Nanoscope IIIA atomic force microscope with a Dimension 3100 controller (Veeco Metrology Inc., Santa Barbara, CA) operating in tapping mode using sharp diamond probes (series DP15, MikroMasch USA, San Jose, CA). Scanning parameters varied with individual tips and samples, but typical values were as follows: set point, 1.1−1.3 V; tapping frequency, 290−330 kHz; scan rate, 1 Hz. The AFM image processing and analysis were performed using ImageJ (*29*).

RESULTS AND DISCUSSION

The Morphology of Aβ(1−40) Aggregates Is Altered by the Cu(II) Ion Concentration in NEM Buffer. We have already demonstrated a direct correlation between the overall morphology of Aβ(1−40) aggregates and the specific Cu(II) coordination in the Aβ(1−40) aggregates in our previous work (*22*). The ESR results were all obtained from Aβ(1−40)

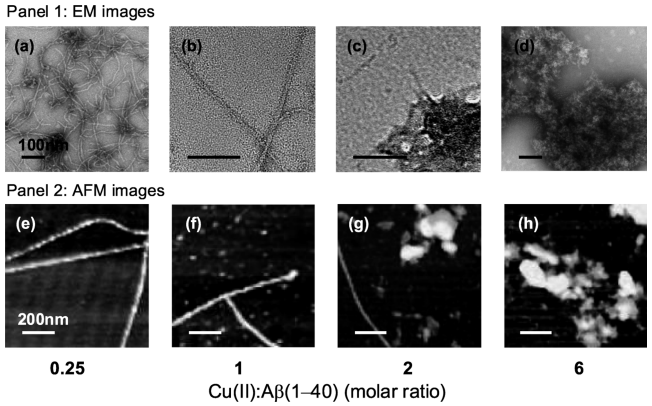

FIGURE 1: (a−d) TEM images of aggregated Aβ(1−40) with Cu(II):Aβ ratios of (a) 0.25:1, (b) 1:1, (c) 2:1, and (d) 6:1. The scale bar is 100 nm. (e−h) Corresponding AFM images of aggregated Aβ(1−40) with Cu(II):Aβ ratios of (e) 0.25:1, (f) 1:1, (g) 2:1, and (h) 6:1. The scale bar is 200 nm. The aggregates were prepared in NEM buffer, and the images suggest a significant increase in the proportion of granular amorphous aggregates as the concentration of Cu(II) is increased.

in Tris buffer, which might contain a signal from aqueous Cu(II). To investigate the effect of buffer on the overall morphology and the ESEEM signal of Aβ(1−40), we prepared the peptide samples in *N*-ethylmorpholine (NEM) and compared the data with those collected in Tris buffer. It is known that NEM buffer minimizes the ESR signal from aqueous Cu(II) ions at neutral pH (~7.4) (*30*).

The overall morphology of mature aggregated Aβ(1−40) in NEM buffer was examined by high-resolution transmission electron microscopy (TEM) and atomic force microscopy (AFM) imaging. To prepare aggregates, Aβ(1−40) was incubated at 37 °C for 5−6 days in the presence of an appropriate Cu(II) concentration. In the presence of an equimolar or subequimolar amount of Cu(II), the peptide exclusively forms fibrillar precipitates that have an extensive nonbranching linear shape. Representative fibril images are shown in panels a and b of Figure 1 (TEM images) and panels e and f of Figure 1 (AFM images). Figure 1d (TEM image) and Figure 1h (AFM image) show the Aβ(1−40) aggregates at a Cu(II):Aβ molar ratio of 6:1. At this Cu(II) ion concentration, only amorphous aggregates rather than well-ordered fibrils exist. When the peptide was prepared with a Cu(II):Aβ molar ratio of 2:1, both linear fibrils and granular amorphous aggregates were observed (cf. Figure 1c,g). Note that in Figure 1g the fibril structure is not as clear as the Aβ fibrils in Figures 1e,f because the amorphous aggregates have relatively greater heights than the fibrils. These images suggest that the change in the morphology of aggregated Aβ(1−40) in NEM buffer, with an increasing Cu(II) ion concentration, is quite similar to that of the Aβ in Tris buffer, which has been reported previously (*22*).

The use of AFM complements imaging by TEM and has an advantage in that samples do not have to be either stained with heavy metals or visualized under high-vacuum conditions. In particular, AFM directly provides three-dimensional images whereas TEM of negatively stained specimens provides projection images that cannot show the detailed three-dimensional morphology of the objects being studied. With this advantage, we have examined the topology of the fibril formed by Aβ(1−40) with a Cu(II):Aβ molar ratio of 1:1 using tapping-mode AFM. Figure 2 shows the AFM image of the helical fibril from

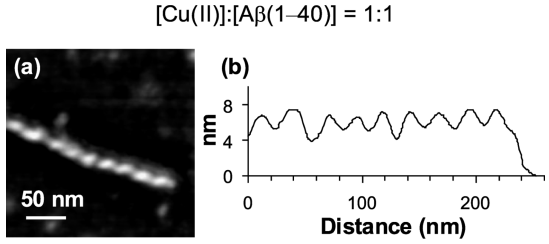

FIGURE 2: (a) AFM image of a helical fibril from Aβ(1−40) at a Cu(II):Aβ ratio of 1:1. (b) Fibril height profile along the fibril axis, showing the regular height variations from the pitch of the fibril with a single repeat period of approximately 25 nm.

Aβ(1−40), demonstrating a clearly periodic substructure in the fibril. In a recent paper, Addadi and co-workers determined the fibril handedness for three disease-related amyloids, including Aβ(1−40), using scanning electron microscopy (SEM) and cryo-SEM (*31*). They found that amyloids of Aβ(1−40) invariably form left-handed helical fibrils. Here, we performed AFM to examine whether Cu(II) ions affect the handedness of amyloid fibrils. We observed the suprastructure of a helical fibril from Aβ(1−40) at a Cu(II):Aβ molar ratio of 1:1. Aβ(1−40) fibrils were characterized by a clearly periodic substructure, spaced at intervals of approximately 25 nm along the Aβ fibril axis (cf. Figure 2b). As reported earlier, the difference between the maximum and minimum heights along the axis in the substructure is at least 1 nm (*32*, *33*). The fibril has a height of ~7 nm and a width of ~40 nm. For Aβ(1−40) with Cu(II), the fibril helicity is left-handed, showing that the helix handedness of the peptide is not affected by Cu(II). Recently, scientists have exploited the amyloidogenic property of Aβ in assembling metallic nanowires (*34*−*36*). The formation of fibrils even in the presence of Cu(II) implies that Aβ might be used as a template for the formation of copper nanowires under an appropriate condition.

ESEEM Spectra of Aβ(1−40) Aggregates Are Dependent on the Cu(II) Ion Concentration. We performed ESEEM experiments on Aβ(1−40) samples containing varying concentrations of Cu(II). ESEEM spectroscopy measures weak hyperfine and quadrupole interactions of the nuclei in the environment (within ~10 Å) of the paramagnetic center (*30*, *37*, *38*). Three-pulse ESEEM spectra of mature aggregated Aβ(1−40) at Cu(II):peptide ratios of (a) 0.25:1, (b) 1:1, (c) 2:1, and (d) 4:1 in NEM buffer are shown in Figure 3. All spectra show three narrow peaks at ~0.55, ~1.04, and ~1.46 MHz and a broad peak centered at ~4.4 MHz. With an increasing Cu(II) ion concentration, a peak at 14.3 MHz also emerges. The three peaks at 0.55, 1.04, and 1.46 MHz are characteristic of a weakly coupled ^{14}N nucleus where the nuclear Zeeman and electron−nuclear hyperfine interaction approximately cancel one another out. Therefore, the energy level splittings are almost completely determined by the ^{14}N nuclear quadrupole interaction (NQI) (*38*−*40*). The ESEEM frequencies for these three transitions are given by (*39*)

$$\nu_0 = \frac{2\eta e^2 qQ}{4h};\ \nu_- = \frac{e^2 qQ(3-\eta)}{4h};\ \nu_+ = \frac{e^2 qQ(3+\eta)}{4h} \quad (1)$$

where e is the electron charge, q is the z-component of the electric field gradient across the nucleus, Q is the ^{14}N nuclear quadrupole moment, η is the asymmetry parameter, and h is Planck's constant. Use of eq 1 to determine the nuclear quadrupole parameters, e^2qQ/h and η, yields values of 1.67 ± 0.08 MHz and 0.66 ± 0.03, respectively.

The broader spectral line at ~4.4 MHz arises from the condition in which the nuclear Zeeman and electron−nuclear hyperfine interactions are additive. This frequency is due to a double-quantum (DQ) transition of the remote nitrogen of the imidazole (*30*, *38*, *41*). Together, the frequencies at or around 0.55, 1.04, and 1.46 MHz as well as the nuclear quadrupole parameters are consistent with histidine coordination.

Several groups have demonstrated that the copper-binding site in Aβ is coordinated by at least two histidine residues (*13*, *14*, *20*, *24*). When the electron spin of the Cu(II) ion interacts with more than one imidazole, the combination frequencies of the three NQI lines may be observed (*30*, *38*, *42*−*44*). These peaks, however, have a weak intensity which can be difficult to measure, especially in the magnitude mode on samples that display a high degree of heterogeneity (*42*). In Figure 3, combination peaks are not clearly seen, which is consistent with our results on truncated sequences of Aβ (*13*). This does not, by itself, rule out the possibility of two or more Cu(II)-coordinating histidine residues (*42*).

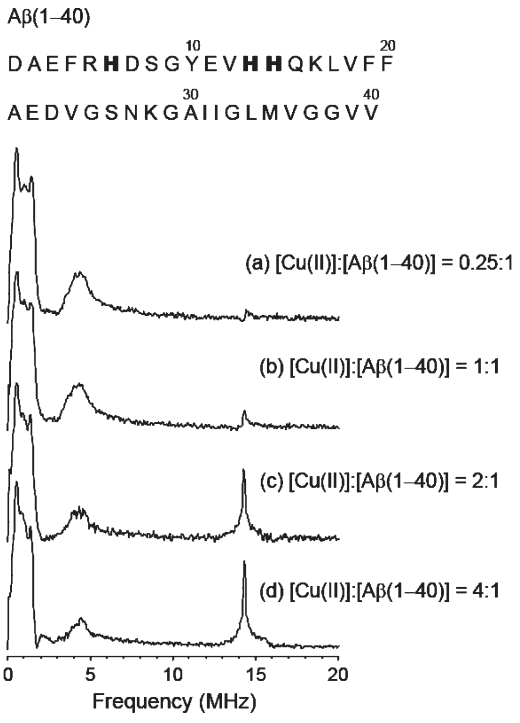

FIGURE 3: Amino acid sequence for Aβ(1−40) and three-pulse ESEEM spectra of aggregated Aβ(1−40) in NEM buffer. The data were collected at Cu(II):peptide ratios of (a) 0.25:1, (b) 1:1, (c) 2:1, and (d) 4:1. Peptide concentrations were 300 μM in all experiments.

At higher Cu(II) ion concentrations, another peak in the ESEEM spectra for Aβ(1−40) with Cu(II) ions is present at 14.3 MHz. This peak is characteristic of interactions between the unpaired electron and proton spins. In Figure 3, the proton ESEEM peak may result from the interaction of the Cu(II) ion with remote hydrogen atoms or the axially coordinated water (*39*).

The fundamental peaks from the ESEEM spectra of Aβ(1−40) with Cu(II) ions in NEM buffer are similar to those in Tris buffer, which are described in our previous work (*22*). The ESEEM spectra of Aβ(1−40) in Tris buffer become broad and heterogeneous as the Cu(II):Aβ molar ratio increases (*22*). The ESEEM spectra of Aβ(1−40) in the NEM buffer show that the intensity of the DQ transition peak at 4.4 MHz is decreased as the Cu(II) ion concentration increases. This result may suggest that the initial multi-histidine coordination for the copper-binding site on the N-terminal region of Aβ(1−40) (cf. Figure 3) may be breaking up at a higher Cu(II) concentration because the height of the 4.4 MHz line is proportional to the number of interacting ^{14}N nuclei (*43*). In addition, the proton ESEEM intensity at 14.3 MHz is significantly attenuated relative to that of Aβ(1−40) with Cu(II) ions in Tris buffer at a higher Cu(II) concentration.

Figure 4 shows the HYSCORE spectra for Aβ(1−40) assembled at Cu(II):peptide ratios of (a) 1:1 and (b) 2:1. Hyperfine sublevel correlation spectroscopy is a two-dimensional ESEEM technique and provides enhanced resolution of ESEEM spectra that may have broadened lines (*45*−*47*). As previously assigned in the three-pulse ESEEM spectra, the NQI and DQ transitions for the remote nitrogen of histidine imidazole are obtained. In addition, cross-peaks, (ν_-, ν_{dq}) and (ν_+, ν_{dq}), are observed due to the correlations between the imidazole ^{14}N NQI and DQ transitions for both spectra. The cross-peaks for Aβ(1−40) at a Cu(II):Aβ molar ratio of 2:1 are more diffuse, suggesting a more heterogeneous copper binding environment at the higher Cu(II) concentration.

Characterization of the Origin of the Proton ESEEM Peak. Recently, our group has reported the ESEEM spectra of Aβ(1−16) with three different molar ratios of Cu(II) ions to the peptide in NEM buffer (*13*). The ESEEM spectra of Aβ(1−16) are quite similar to those of aggregated Aβ(1−40) with an equimolar or subequimolar amount of Cu(II). The spectra show the three NQI peaks below 2 MHz and a broad DQ transition peak at ~4 MHz, indicating that histidine residues coordinate to

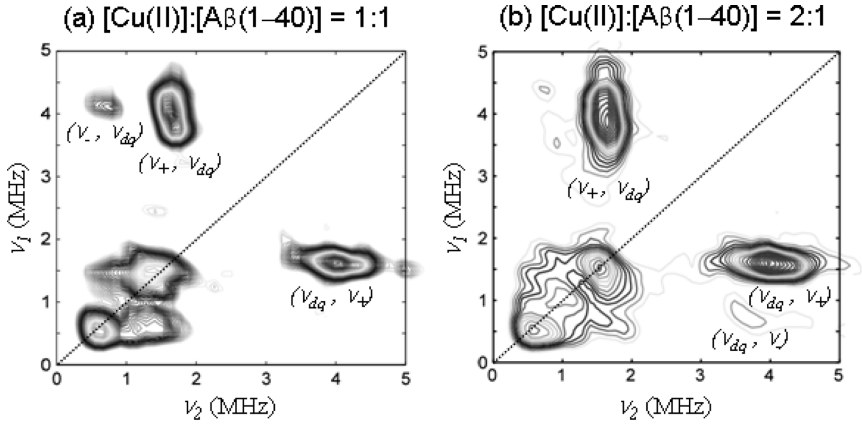

FIGURE 4: HYSCORE spectra of aggregated Aβ(1−40) at Cu(II):peptide ratios of (a) 1:1 and (b) 2:1. The spectra show the correlations between the imidazole ^{14}N nuclear quadrupolar and double-quantum transitions.

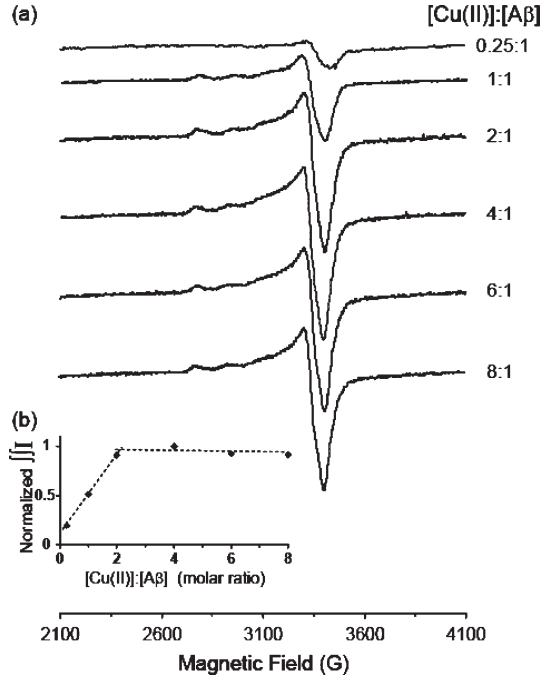

FIGURE 5: (a) CW ESR spectra obtained at Cu(II):Aβ(1−40) ratios of 0.25:1, 1:1, 2:1, 4:1, 6:1, and 8:1. (b) Double integration of ESR spectra plotted vs the molar ratio of Cu(II) ions to peptide, indicating two Cu(II) ions binding a single Aβ(1−40). The maximum point of the data was normalized to 1.

Cu(II) in both Aβ(1−16) and Aβ(1−40). Aβ(1−16) does not form aggregates and has a soluble form, which is a highly flexible monomer. Therefore, the almost unchanged ESEEM spectra from Aβ(1−16) and the aggregated Aβ(1−40) at an equimolar or subequimolar Cu(II):Aβ ratio suggest that the Aβ fibrils are able to bind Cu(II) ions with a coordination geometry identical to that of monomeric Aβ (*11*, *24*, *48*). Recently, fluorescence quenching and circular dichroism experiments have revealed that the binding affinity of Cu(II) for the monomeric and fibrillar forms is almost identical. These results also suggest that fibrillar Aβ has the same Cu(II) coordination geometry as monomeric Aβ (*12*).

When Aβ(1−16) was prepared at a high Cu(II) ion concentration [at a Cu(II):Aβ(1−16) ratio of 4:1], the ESEEM spectrum is almost identical to that of the peptide in the presence of equimolar or subequimolar Cu(II) (*13*), indicating that the primary copper-binding site in Aβ(1−16) is preserved and not significantly affected by the Cu(II) ion concentration (*12*). These ESEEM results do not, by themselves, rule out a second copper-binding site in Aβ(1−16), especially if the second site primarily involves oxygen ligands from aspartate and/or glutamate and non-imidazole nitrogen ligands, which has been suggested by Viles and co-workers (*12*). Also, our CW ESR experimental results for Aβ(1−16) are consistent with their work in that at least two components are present at greater than equimolar Cu(II) concentrations (data not shown). However, the ESEEM results on Aβ(1−16) are in contrast to those of Aβ(1−40), for which the 14.3 MHz proton ESEEM peak in the ESEEM spectra increase at greater than equimolar Cu(II) ion concentrations (cf. Figure 3c,d).

To confirm additional copper-binding sites in aggregated Aβ(1−40), we collected continuous wave (CW) ESR spectra at Cu(II):peptide ratios of 0.25:1, 1:1, 2:1, 4:1, 6:1, and 8:1 (cf. Figure 5a). Double integration of the first-derivative CW ESR spectra was used to identify the number of Cu(II) ions binding to the peptide. As shown in Figure 5b, the magnitude of the signal increases linearly and plateaus at 2 equiv of Cu(II) ions. No significant increase in the intensity of the CW ESR spectrum of Aβ(1−40) at a Cu(II):Aβ ratio of 8:1 is observed. Free Cu(II) ions have a dramatically attenuated ESR signal relative to the Cu(II) bound to Aβ in NEM buffer at pH 7.4 (*20*, *29*). Therefore, these data show that Aβ(1−40) binds two Cu(II) ions. A second set of Cu(II) hyperfine peaks at a Cu(II):Aβ(1−40) ratio of 2:1 is observed, and this may be additional evidence of the second copper-binding site in Aβ(1−40). Szalai and co-workers have also reported a second component in CW ESR spectra for both soluble and fibrillar Aβ(1−40) (*24*). Bush and co-workers have demonstrated two cooperative copper-binding sites in Aβ(1−40) at pH 7.4 (*21*). A second copper-binding site of Aβ(1−42) has been revealed in the presence of methanol (20%, v/v) by Viles and co-workers (*12*). They have suggested that alcohols such as methanol disturb tertiary interactions of the hydrophobic tail and expose some residues that would otherwise be cryptic or hidden (*12*, *49*). In the previous paper, they also demonstrated that Aβ(1−28) has two copper-binding sites for a single peptide (*20*).

It is certain that the ESR data are representative of bound copper ions, based on a variety of factors. Different binding affinities of Cu(II) for Aβ peptide, ranging from micromolar to attomolar, have been reported (*50*, *51*). To gain information about the fraction of Cu(II) bound to Aβ at equimolar concentrations, the double-integrated intensities of CW ESR spectra obtained at different concentrations, including 300, 150, and 75 μM, were compared (data not shown). The double integration is almost proportional to the concentration, signifying that the fraction of Cu(II) bound to Aβ is not significantly affected by dilution. Also, it is certain that the fraction is greater than 83% for the 300 μM sample even if the dissociation constant is the largest reported value (~10 μM) for the first binding site (*50*). The dissociation constant of the second binding site has been reported to be on the order of 10 μM (*51*).

The ESEEM and CW ESR results, taken together, indicate that there are two binding sites at high Cu(II) ion concentrations. The binding site for the first molar equivalent of Cu(II) ions is definitely located on the N-terminal region of the peptide, which includes three histidine residues. On the other hand, the second binding site is significantly associated with hydrogen atom(s) (cf. Figure 3c,d).

To further investigate the second copper-binding site in Aβ(1−40) and to determine whether the proton ESEEM peak is due to the interaction with solvent protons, the ESEEM spectra were collected on aggregated Aβ(1−40) prepared in D_2O. Figure 6 shows three-pulse ESEEM spectra for Aβ(1−40) assembled with a Cu(II):peptide ratio of 2:1 in (a) H_2O and (b) D_2O.

The large 14.3 MHz proton ESEEM peak was eliminated when the solvent was switched to D_2O, and a new peak was observed at ~2 MHz as shown in Figure 6b. The 2 MHz peak arises from the interaction between deuterium nuclei and the unpaired electron of the Cu(II) ion. The analysis of the ESEEM spectrum with the peptide in D_2O indicates that the second copper-binding site in Aβ(1−40) is in the proximity of water or solvent-exchangeable peptide protons. This result is consistent with work by Faller and co-workers (*51*). In addition, a small proton ESEEM peak at 14.3 MHz still remains, which suggests that water may not be the sole source of the oxygen donor in 3N1O Cu(II) coordination in the equatorial plane. Szalai and co-workers also supported the possibility that water is not an

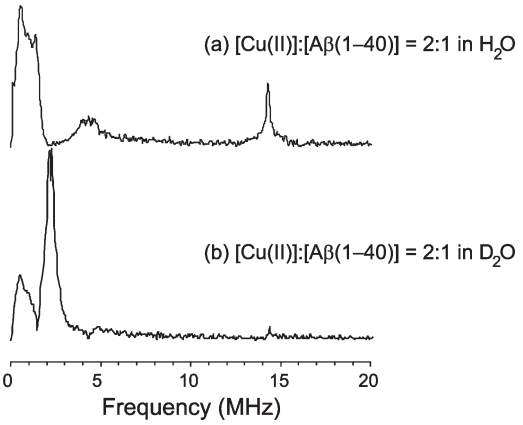

FIGURE 6: Three-pulse ESEEM spectra of Aβ(1−40) assembled with a Cu(II):peptide ratio of 2:1 in (a) H_2O and (b) D_2O. The 14.3 MHz proton ESEEM peak is strongly attenuated, and the deuterium ESEEM peak is observed near 2 MHz in spectrum b.

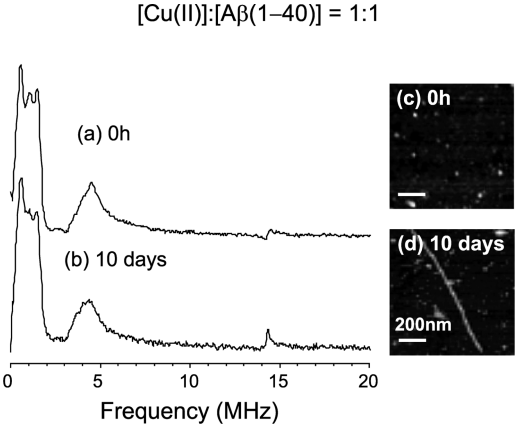

FIGURE 7: (a and b) Three-pulse ESEEM spectra of Aβ(1−40) at a Cu(II):Aβ molar ratio of 1:1 at incubation times of (a) 0 h (an initial state) and (b) 10 days (a fully aggregated state) in NEM buffer. (c and d) AFM images of Aβ(1−40) at incubation times of (c) 0 h and (d) 10 days.

equatorial ligand to the Cu(II) ion using CW ESR with the substitution of $H_2{}^{16}O$ with $H_2{}^{17}O$ (*52*).

Incubation Time Dependence of the ESEEM Spectra for Aβ(1−40) with Cu(II) Ion. We investigated the incubation time dependence of the ESEEM spectra for Aβ(1−40) at Cu(II):Aβ(1−40) molar ratios of 1:1 and 2:1. Figure 7 shows the ESEEM spectra (a and b) and AFM images (c and d) for Aβ(1−40) at a Cu(II):Aβ(1−40) ratio of 1:1 sampled at 0 h (an initial state) and 10 days (a fully aggregated state). At 0 h, Aβ(1−40) forms dispersed monomers or oligomers, with a very weak ThT fluorescence signal (cf. below and Figure 9). After 10 days, the AFM image for Aβ(1−40) aggregates shows mature fibrils (cf. Figure 7d). However, there are no significant differences in the peak positions, shapes, or intensities in the ESEEM spectra between monomeric and fibrillar Aβ(1−40), supporting again the possibility that the copper coordination environments in Aβ(1−40) between monomers and mature fibrils are not dramatically different from each other (*11*, *12*).

In contrast, the ESEEM spectra for Aβ(1−40) at a Cu(II):Aβ(1−40) ratio of 2:1 have a significant difference in the proton ESEEM peak at 14.3 MHz between the incubation times of 0 h (Figure 8a) and 10 days (Figure 8b). At 0 h, Aβ(1−40) at a Cu(II):Aβ(1−40) ratio of 2:1 exhibits the same ESEEM spectrum as

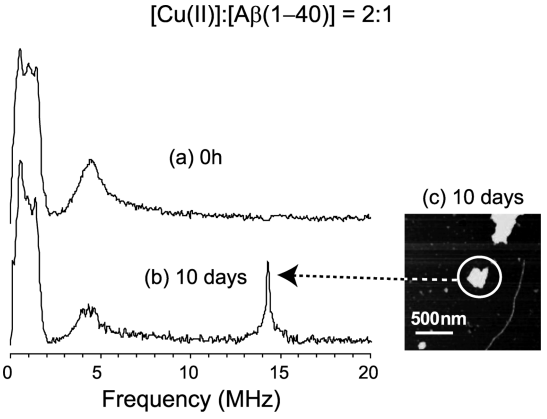

FIGURE 8: Three-pulse ESEEM spectra of Aβ(1−40) at a Cu(II):Aβ molar ratio of 2:1 at incubation times of (a) 0 h (an initial state) and (b) 10 days (a fully aggregated state) in NEM buffer. The proton ESEEM peak at 14.3 MHz emerges in spectrum b. (c) After 10 days, mature fibrils and amorphous aggregates are observed together in an AFM image.

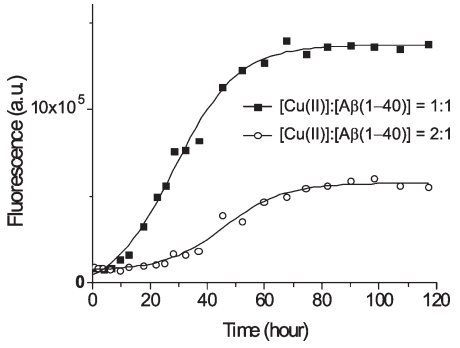

FIGURE 9: Thioflavin T (ThT) fluorescence assays for Aβ(1−40) at Cu(II):Aβ ratios of 1:1 (■) and 2:1 (○) as function of time. An increase in the lag time and a decrease of the amyloid fibril contents are observed at a Cu(II):Aβ ratio of 2:1.

Aβ(1−40) at a ratio of 1:1 at 0 h, suggesting that the peptide also exists as monomers or oligomers at the initial point (cf. Figure 8a). After 10 days, however, a proton ESEEM peak at 14.3 MHz emerges while the ^{14}N ESEEM peaks below 3 MHz remain practically unchanged, which implies that the second copper-binding site is exposed to a proton-rich condition. In addition, the AFM image for Aβ(1−40) aggregates after 10 days shows mature fibrils and amorphous aggregates together, as shown in Figure 8c. Although our results suggest that the second copper-binding site in Aβ(1−40) is exposed to a proton-rich environment, the structure of the binding site is not yet clear and could be elusive to determine because the binding site may form during the aggregation of the peptide.

The process of fibril formation involves the interpeptide interaction between two β-sheets in the peptide. At an equimolar Cu(II):Aβ(1−40) ratio, the Cu(II) ion is coordinated with histidine residues on the flexible N-terminal region of Aβ (*13*, *14*), providing the characteristic frequencies in the ESEEM spectrum. Therefore, this copper-binding site is not involved with the β-sheet core region and may not affect the interpeptide interaction in forming a fibril. On the other hand, Aβ(1−40) at a Cu(II):peptide ratio of 2:1 has the second weaker copper-binding site (CW ESR data shown in Figure 5) and the site is exposed to water or exchangeable protons on the peptide [ESEEM with Aβ(1−40) in D_2O shown in Figure 6]. The second

copper-binding site could interfere with the interpeptide interaction in Aβ(1−40), leading to nonfibrillar amorphous aggregates (AFM image shown in Figure 8c). Interestingly, Dawson and co-workers have shown that some nanoparticles also inhibit the fibrillization of Aβ by affecting the nucleation step in a concentration-dependent manner (*53*). Thus, it is probable that a relatively high concentration of Cu(II) ions also alters the conformational transition while the nucleation occurs.

Effect of Cu(II) Ions on the Formation of Fibrils or Amorphous Aggregates in Aβ(1−40). A simple quantitative analysis for the difference between Aβ(1−40) at Cu(II):Aβ ratios of 1:1 and 2:1 is described in terms of the formation of mature fibrils and amorphous aggregates in Aβ(1−40), respectively. To further investigate this interpretation of the data, we performed a ThT fluorescence assay and a CD experiment.

ThT is a fluorescent dye that specifically binds with the cross-β-pleated sheets of amyloid structures (*54*, *55*). As shown in Figure 9, the fluorescence of ThT for Aβ(1−40) at both Cu(II):Aβ ratios of 1:1 (■) and 2:1 (○) shows a sigmoidal increase with time. The lag time of the reaction is increased with Aβ(1−40) at a Cu(II):Aβ ratio of 2:1, and the time to proceed to a steady level of fluorescence is also increased with an increase in Cu(II) ion concentration. The final equilibrium level is decreased in Aβ(1−40) at a Cu(II):Aβ ratio of 2:1, indicating that Cu(II) ions may inhibit the fibril formation of the peptide. In Figure 1, at a Cu(II):Aβ ratio of 1:1, the TEM and AFM images show the only fibrils that have a linear shape. At a Cu(II):Aβ ratio of 2:1, Aβ(1−40) forms two distinct types of morphologies, linear fibrils and amorphous aggregates. Together, these data suggest that a process that forms granular amorphous aggregates with Cu(II) ions may interfere with the conversion into the fibrillar form.

Using a different assay to assess the β-sheet structure, UV CD spectroscopy, the secondary structure of Aβ(1−40) at two different Cu(II) ion concentrations was monitored. Figure 10a shows the CD spectra of Aβ(1−40) at a Cu(II):Aβ molar ratio of 1:1 sampled at an initial state (dashed line) and a fully aggregated state (solid line). The first spectral curve after fibrils have begun to form has a minimum mean residue ellipticity at ∼200 nm, indicating that the secondary structure of Aβ(1−40) is a random coil at an initial state (*56*, *57*). At a fully aggregated state of Aβ(1−40), the CD spectrum has a minimum at ∼215 nm, which is characteristic of the β-sheet structure (*58*, *59*). To examine the conformation with an increased level of β-sheet for Aβ(1−40) at Cu(II):Aβ ratios of 1:1 and 2:1 as a function of time, we monitored a single wavelength, 215 nm. As shown in Figure 10b, Aβ(1−40) develops the β-sheet secondary structure at a Cu(II):Aβ ratio of 1:1, supported by a negatively increased mean residue ellipticity at 215 nm in the spectrum. Interestingly, the signal intensity of Aβ(1−40) at 2 molar equiv of Cu(II) ions to the peptide at 215 nm has a large negative value from the initial point and does not change with time, suggesting that a relatively large amount of β-sheet conformation remains unchanged from the initial state to the end of the aggregation process. Using CD spectroscopy, Viles and co-workers have also demonstrated that the secondary structure of the main chain in Aβ becomes more ordered as the Cu(II):peptide ratio increases (*20*). While the CD data can be affected by light scattering caused by large aggregates, the use of a short path length cuvette (0.1 cm) is expected to reduce the chance of scattering. It is also unlikely that the overall qualitative trend in the spectra is significantly altered by light scattering since significant changes are observed over the entire scanned spectral region. The CD data are thus valuable for the qualitative examination of conformational change.

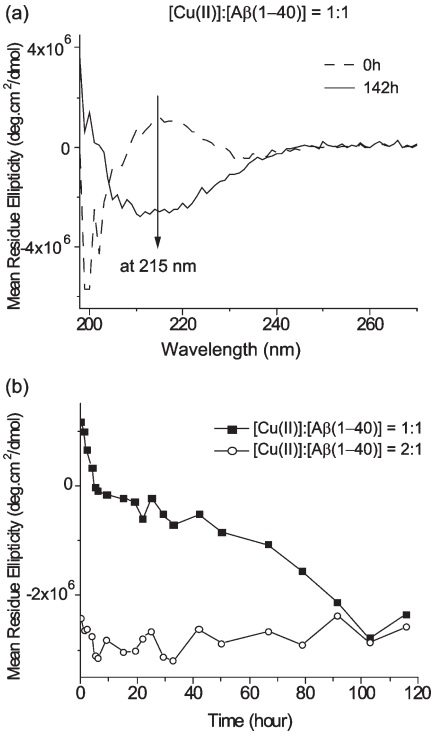

FIGURE 10: (a) UV CD spectra of Aβ(1−40) at a Cu(II):Aβ ratio of 1:1 over time. (b) Mean residue ellipticity at 215 nm as a function of time for Aβ(1−40) at Cu(II):Aβ ratios of 1:1 (■) and 2:1 (○). A decreased mean residue ellipticity at 215 nm indicates the increased level of β-sheet conformation.

The ThT fluorescence assay and CD experiment measure different aspects of amyloid aggregate formation. The ThT assay directly measures only fibril formation because of the specificity of ThT for amyloid structures; neither monomeric Aβ nor amorphous aggregates significantly enhance the emission intensity of ThT. On the other hand, the CD experiment independently measures the formation of β-sheet structures irrespective of whether the aggregates are amorphous or fibrillar (*60*). When Aβ(1−40) is aggregated at a Cu(II):Aβ ratio of 1:1, the total amount of β-sheet structure is increased (as measured in the CD experiment) and amyloid fibrils are formed (as measured in the ThT assay) as a function of time. When Aβ(1−40) is aggregated at a Cu(II):Aβ ratio of 2:1, there is a significant amount of β-sheet structure that forms immediately, although there are few amyloid fibrils in the initial part of fibril formation (as measured in the ThT assay or by AFM and TEM). Therefore, in this case, Cu(II) ions induce the aggregates that have the nonfibrillar β-sheet conformation and interfere with the conformational transition into amyloid fibrils.

SUMMARY

When Aβ(1−40) was prepared in NEM buffer, the AFM and TEM images demonstrated that the aggregation ability of Aβ(1−40) with Cu(II) ions is similar to that of the peptide in Tris buffer. At low concentrations of Cu(II), the aggregates are fibrillar in shape. The presence of Cu(II) ions does not affect the handedness of the Aβ(1−40) helical fibril. At greater than equimolar concentrations of Cu(II) ions, amorphous aggregates result. The ESEEM data for aggregates of Aβ(1−40) in NEM buffer show that as the Cu(II) ion concentration increases the

magnitude of the double-quantum ^{14}N ESEEM peak at 4.4 MHz is decreased and the proton ESEEM peak at 14.3 MHz appears. At an equimolar Cu(II):Aβ(1−40) ratio, the Cu(II) ion is coordinated with multi-histidine residues in both monomeric and fibrillar Aβ. The initial copper-binding site breaks up at higher copper concentrations, and a second site that is solvent exposed begins to emerge. In addition, the CW ESR data demonstrate two copper-binding sites in Aβ(1−40). The proton ESEEM peak in Aβ(1−40) at a Cu(II):Aβ ratio of 2:1 was further investigated as the second copper-binding site. The ESEEM experiment with Aβ(1−40) in D_2O suggests that the second copper-binding site is in the vicinity of water or exchangeable peptide protons. Therefore, the proton ESEEM peaks may be significantly involved in the granular amorphous aggregates of Aβ(1−40), which are shown in the AFM image. ThT fluorescence data also exhibit a weakened ability to form Aβ(1−40) fibrils with 2 equiv of Cu(II) ions added to the peptide. Taken together, these results suggest that the second copper-binding site in Aβ(1−40) is in the proton-rich environment and interferes with the interpeptide interaction between two different peptide β-sheets, leading to granular amorphous aggregates of the peptide.

ACKNOWLEDGMENT

We thank the Peterson Institute of Nanoscience and Engineering for access to a high-resolution field emission transmission electron microscope. We also thank the reviewers for help with the interpretation of some of the changes observed in the ESEEM data.

REFERENCES

1. Hardy, J., and Selkoe, D. J. (2002) The amyloid hypothesis of Alzheimer's disease: Progress and problems on the road to therapeutics. *Science 297*, 353–356.
2. McLaurin, J., and Chakrabartty, A. (1996) Membrane Disruption by Alzheimer β-Amyloid Peptides Mediated through Specific Binding to either Phospholipids or Gangliosides: Implications for Neurotoxicity. *J. Biol. Chem. 271*, 26482–26489.
3. Walsh, D. M., Lomarkin, A., Benedek, G. B., and Condron, M. M. (1997) Amyloid-β protein fibrillogenesis. *J. Biol. Chem. 272*, 22364–22372.
4. Lambert, M. P., Barlow, A. K., Chromy, B. A., Edwards, C., Freed, R., Liosatos, M., Morgan, T. E., Rozovsky, I., Trommer, B., Viola, K. L., Wals, P., Zhang, C., Finch, C. E., Krafft, G. A., and Klein, W. L. (1998) Diffusible, Nonfibrillar Ligands Derived from Aβ_{1-42} are Potent Central Nervous System Neurotoxins. *Proc. Natl. Acad. Sci. U.S.A. 95*, 6448–6453.
5. Carrotta, R., Manno, M., Bulone, D., Martorana, V., and San Biagio, P. L. (2005) Protofibril Formation of Amyloid β-Protein at Low pH via a Non-cooperative Elongation Mechanism. *J. Biol. Chem. 280*, 30001–30008.
6. Miura, T., Suzuki, K., Kohata, N., and Takeuchi, H. (2000) Metal Binding Modes of Alzheimer's Amyloid-β Peptide in Insoluble Aggregates and Soluble Complexes. *Biochemistry 39*, 7024–7031.
7. Yoshiike, Y., Tanemura, K., Murayama, O., Akagi, T., Murayama, M., Sato, S., Sun, X., Tanaka, N., and Takashima, A. (2001) New Insights on How Metals Disrupt Amyloid β-Aggregation and Their Effects on Amyloid-β Cytotoxicity. *J. Biol. Chem. 276*, 32293–32299.
8. Raman, B., Ban, T., Yamaguchi, K. I., Sakai, M., Kawai, T., Naiki, H., and Goto, Y. (2005) Metal Ion-dependent Effects of Clioquinol on the Fibril Growth of an Amyloid β Peptide. *J. Biol. Chem. 280*, 16157–16162.
9. Atwood, C. S., Moir, R. D., Huang, X., Scarpa, R. C., Bacarra, N. M. E., Romano, D. M., Hartshorn, M. A., Tanzi, R. E., and Bush, A. I. (1998) Dramatic Aggregation of Alzheimer Aβ by Cu(II) Is Induced by Conditions Representing Physiological Acidosis. *J. Biol. Chem. 273*, 12817–12826.
10. Zou, J., Kajita, K., and Sugimoto, N. (2001) Cu^{2+} Inhibits the Aggregation of Amyloid β-Peptide(1−42) in vitro. *Angew. Chem., Int. Ed. 40*, 2274–2277.
11. Karr, J. W., Kaupp, L. J., and Szalai, V. A. (2004) Amyloid-β Binds Cu^{2+} in a Mononuclear Metal Ion Binding Site. *J. Am. Chem. Soc. 126*, 13534–13538.
12. Sarell, C. J., Syme, C. D., Rigby, S. E. J., and Viles, J. H. (2009) Copper(II) Binding to Amyloid-β Fibrils of Alzheimer's Disease Reveals a Picomolar Affinity: Stoichiometry and Coordination Geometry Are Independent of Aβ Oligomeric Form. *Biochemistry 48*, 4388–4402.
13. Shin, B.-k., and Saxena, S. (2008) Direct Evidence That All Three Histidine Residues Coordinate to Cu(II) in Amyloid-β_{1-16}. *Biochemistry 47*, 9117–9123.
14. Drew, S. C., Noble, C. J., Masters, C. L., Hanson, G. R., and Barnham, K. J. (2009) Pleomorphic Copper Coordination by Alzheimer's Disease Amyloid-β Peptide. *J. Am. Chem. Soc. 131*, 1195–1207.
15. Hilbich, C., Kisters-Woike, B., Reed, J., Masters, C. L., and Beyreuther, K. (1992) Substitutions of hydrophobic amino acids reduce the amyloidogenicity of Alzheimer's disease βA4 peptides. *J. Mol. Biol. 228*, 460–473.
16. Soreghan, B., Kosmoski, J., and Glabe, C. (1994) Surfactant properties of Alzheimer's Aβ peptides and the mechanism of amyloid aggregation. *J. Biol. Chem. 269*, 28551–28554.
17. Benzinger, T. L. S., Gregory, D. M., Burkoth, T. S., Miller-Auer, H., Lynn, D. G., Botto, R. E., and Meredith, S. C. (2000) Two-Dimensional Structure of β-Amyloid(10−35) Fibrils. *Biochemistry 39*, 3491–3499.
18. Lu, K., Jacob, J., Thiyagarajan, P., Conticello, V. P., and Lynn, D. G. (2003) Exploiting Amyloid Fibril Lamination for Nanotube Self-Assembly. *J. Am. Chem. Soc. 125*, 6391–6393.
19. Gordon, D. J., Balbach, J. J., Tycko, R., and Meredith, S. C. (2004) Increasing the Amphiphilicity of an Amyloidogenic Peptide Changes the β-Sheet Structure in the Fibrils from Antiparallel to Parallel. *Biophys. J. 86*, 428–434.
20. Syme, C. D., Nadal, R. C., Rigby, S. E. J., and Viles, J. H. (2004) Copper Binding to the Amyloid-β (Aβ) Peptide Associated with Alzheimer's Disease. *J. Biol. Chem. 279*, 18169–18177.
21. Atwood, C. S., Scarpa, R. C., Huang, X., Moir, R. D., Jones, W. D., Fairlie, D. P., Tanzi, R. E., and Bush, A. I. (2000) Characterization of Copper Interactions with Alzheimer Amyloid β Peptides: Identification of an Attomolar-Affinity Copper Binding Site on Amyloid β1−42. *J. Neurochem. 75*, 1219–1233.
22. (a) Jun, S., and Saxena, S. (2007) The aggregated state of amyloid-β peptide in vitro depends on Cu^{2+} concentration. *Angew. Chem., Int. Ed. 46*, 3959–3961. (b) Jun, S., and Saxena, S. (2007) The aggregated state of amyloid-β peptide in vitro depends on Cu^{2+} concentration. *Angew. Chem., Int. Ed. 46*, 5263.
23. Smith, D. P., Ciccotosto, G. D., Tew, D. J., Fodero-Tavoletti, M. T., Johanssen, T., Masters, C. L., Barnham, K. J., and Cappai, R. (2007) Concentration Dependent Cu^{2+} Induced Aggregation and Dityrosine Formation of the Alzheimer's Disease Amyloid-β Peptide. *Biochemistry 46*, 2881–2891.
24. Karr, J. W., and Szalai, V. A. (2008) Cu(II) Binding to Monomeric, Oligomeric, and Fibrillar Forms of the Alzheimer's Disease Amyloid-β Peptide. *Biochemistry 47*, 5006–5016.
25. Fauth, J. M., Schweiger, A., Braunschweiler, A., Forrer, J., and Ernst, R. R. (1986) Elimination of Unwanted Echoes and Reduction of Dead Time in Three-Pulse Electron Spin-Echo Spectroscopy. *J. Magn. Reson. 66*, 74–85.
26. Gemperle, C., Aebli, G., Schweiger, A., and Ernst, R. R. (1990) Phase Cycling in Pulse EPR. *J. Magn. Reson. 88*, 241–256.
27. Hasegawa, K., Yamaguchi, I., Omata, S., Gejyo, F., and Naiki, H. (1999) Interaction between Aβ(1−42) and Aβ(1−40) in Alzheimer's β-Amyloid Fibril Formation in Vitro. *Biochemistry 38*, 15514–15521.
28. Harris, J. R., and Agutter, P. S. (1970) A negative staining study of human erythrocyte ghosts and rat liver nuclear membranes. *J. Ultrastruct. Res. 33*, 219–232.
29. http://rsb.info.nih.gov/ij.
30. Aronoff-Spencer, E., Burns, C. S., Avdievich, N. I., Gerfen, G. J., Peisach, J., Antholine, W. E., Ball, H. L., Cohen, F. E., Prusiner, S. B., and Millhauser, G. L. (2000) Identification of the Cu^{2+} binding sites in the N-terminal domain of the prion protein by EPR and CD spectroscopy. *Biochemistry 39*, 13760–13771.
31. Rubin, N., Perugia, E., Goldschmidt, M., Fridkin, M., and Addadi, L. (2008) Chirality of amyloid suprastructures. *J. Am. Chem. Soc. 130*, 4602–4603.
32. Wong, S. S., Harper, J. D., Lansbury, P. T., Jr., and Lieber, C. M. (1998) Carbon Nanotube Tips: High-Resolution Probes for Imaging Biological Systems. *J. Am. Chem. Soc. 120*, 603–604.
33. Harper, J. D., Wong, S. S., Lieber, C. M., and Lansbury, P. T., Jr. (1999) Assembly of Aβ amyloid protofibrils: An in vitro model for a

possible early event in Alzheimer's disease. *Biochemistry 38*, 8972–8980.
34. Morgan, D. M., Dong, J., Jacob, J., Lu, K., Apkarian, R. P., Thiyagarajan, P., and Lynn, D. G. (2002) Metal Switch for Amyloid Formation: Insight into the Structure of the Nucleus. *J. Am. Chem. Soc. 124*, 12644–12645.
35. Hamada, D., Yanagihara, I., and Tsumoto, K. (2004) Engineering amyloidogenicity towards the development of nanofibrillar materials. *Trends Biotechnol. 22*, 93–97.
36. Dong, J., Canfield, J. M., Mehta, A. K., Shokes, J. E., Tian, B., Childers, W. S., Simmons, J. A., Mao, Z., Scott, R. A., Warncke, K., and Lynn, D. G. (2007) Engineering metal ion coordination to regulate amyloid fibril assembly and toxicity. *Proc. Natl. Acad. Sci. U.S.A. 104*, 13313–13318.
37. Mims, W. B. (1972) Envelope modulation in spin echo experiments. *Phys. Rev. B 5*, 2409–2419.
38. Mims, W. B., and Peisach, J. (1978) The nuclear modulation effect in electron spin echoes for complexes of Cu^{2+} and imidazole with ^{14}N and ^{15}N. *J. Chem. Phys. 69*, 4921–4930.
39. Dikanov, S. A., Tsvetkov, Y. D., Bowman, M. K., and Astashkin, A. V. (1982) Parameters of Quadrupole Coupling of ^{14}N Nuclei in Chlorophyll a Cations Determined by the Electron Spin Echo Method. *Chem. Phys. Lett. 90*, 149–153.
40. Deligiannakis, Y., Louloudi, M., and Hadjiliadis, N. (2000) Electron spin echo envelope modulation (ESEEM) spectroscopy as a tool to investigate the coordination environment of metal centers. *Coord. Chem. Rev. 204*, 1–112.
41. Burns, C. S., Aronoff-Spencer, E., Dunham, C. M., Lario, P., Avdievich, N. I., Antholine, W. E., Olmstead, M. M., Vrielink, A., Gerfen, G. J., Peisach, J., Scott, W. G., and Millhauser, G. L. (2002) Molecular features of the copper binding sites in the octarepeat domain of the prion protein. *Biochemistry 41*, 3991–4001.
42. Kosman, D. J., Peisach, J., and Mims, W. B. (1980) Pulsed Electron Paramagnetic Resonance Studies of the Cu(II) Site in Galactose Oxidase. *Biochemistry 19*, 1304–1308.
43. McCracken, J., Pember, S., Benkovic, S. J., Villafranca, J. J., Miller, R. J., and Peisach, J. (1988) Electron-Spin-Echo Studies of the Copper Binding Site in Phenylalanine Hydroxylase from *Chromobacterium violaceum*. *J. Am. Chem. Soc. 110*, 1069–1074.
44. Jiang, F., McCracken, J., and Peisach, J. (1990) Nuclear quadrupole interactions in copper(II)-diethylenetriamine-substituted imidazole complexes and in copper(II) proteins. *J. Am. Chem. Soc. 112*, 9035–9044.
45. Ponti, A., and Schweiger, A. (1995) Nuclear Coherence-Transfer Echoes in Pulsed EPR. *J. Chem. Phys. 102*, 5207–5219.
46. Kofman, V., Shane, J. J., Dikanov, S. A., Bowman, M. K., Libman, J., Shanzer, A., and Goldfarb, D. (1995) Coordination of Cu(II) to Lipophilic Bis-hydroxamate Binders As studied by One- and Two-Dimensional Electron Spin Echo Spectroscopy. *J. Am. Chem. Soc. 117*, 12771–12778.
47. Kofman, V., Farver, O., Pecht, I., and Goldfarb, D. (1996) Two-Dimensional Pulsed EPR spectroscopy of the Copper Protein Azurin. *J. Am. Chem. Soc. 118*, 1201–1206.
48. Antzutkin, O. N. (2004) Amyloidosis of Alzheimer's Aβ peptides: Solid-state nuclear magnetic resonance, electron paramagnetic resonance, transmission electron microscopy, scanning transmission electron microscopy and atomic force microscopy studies. *Magn. Reson. Chem. 42*, 231–246.
49. Kony, D. B., Hunenberger, P. H., and van Gunsteren, W. F. (2007) Molecular dynamics simulations of the native and partially folded states of ubiquitin: Influence of methanol cosolvent, pH, and temperature on the protein structure and dynamics. *Protein Sci. 16*, 1101–1118.
50. Tougu, V., Karafin, A., and Palumaa, P. (2008) Binding of zinc(II) and copper(II) to the full-length Alzheimer's amyloid-β peptide. *J. Neurochem. 104*, 1249–1259.
51. Guilloreau, L., Damian, L., Coppel, Y., Mazarguil, H., Winterhalter, M., and Faller, P. (2006) Structural and thermodynamical properties of Cu^{II} amyloid-β16/28 complexes associated with Alzheimer's disease. *J. Biol. Inorg. Chem. 11*, 1024–1038.
52. Karr, J. W., Akintoye, H., Kaupp, L. J., and Szalai, V. A. (2005) N-Terminal Deletions Modify the Cu^{2+} Binding Site in Amyloid-β. *Biochemistry 44*, 5478–5487.
53. Cabaleiro-Lago, C., Quinlan-Pluck, F., Lynch, I., Lindman, S., Minogue, A. M., Thulin, E., Walsh, D. M., Dawson, K. A., and Linse, S. (2008) Inhibition of Amyloid β Protein Fibrillation by Polymeric Nanoparticles. *J. Am. Chem. Soc. 130*, 15437–15443.
54. LeVine, H.III (1993) Thioflavin T interaction with synthetic Alzheimer's disease β-amyloid peptides: Detection of amyloid aggregation in solution. *Protein Sci. 2*, 404–410.
55. Castillo, G. M., Ngo, C., Cummings, J., Wright, T. N., and Snow, A. D. (1997) Perlecan Binds to the β-Amyloid Proteins (Aβ) of Alzheimer's Disease, Accelerates Aβ Fibril Formation, and Maintains Aβ Fibril Stability. *J. Neurochem. 69*, 2452–2465.
56. Holzwarth, G., and Doty, P. (1965) The Ultraviolet Circular Dichroism of Polypeptides. *J. Am. Chem. Soc. 87*, 218–228.
57. Perczel, A., and Hollosi, M. (1996) Turns. In Circular Dichroism and the Conformational Analysis of Biomolecules (Fasman, G. D., Ed.) pp 285−367, Plenum Press, New York.
58. Greendield, N. J. (2006) Using circular dichroism spectra to estimate protein secondary structure. *Nat. Protoc. 1*, 2876–2890.
59. Whitmore, L., and Wallace, B. A. (2008) Protein secondary structure analyses from circular dichroism spectroscopy: Methods and reference databases. *Biopolymers 89*, 392–400.
60. Benseny-Cases, N., Cocera, M., and Cladera, J. (2007) Conversion of non-fibrillar β-sheet oligomers into amyloid fibrils in Alzheimer's disease amyloid peptide aggregation. *Biochem. Biophys. Res. Commun. 361*, 916–921.